Collecting BVR Photometry and Age/Distance Estimates of NGC-7789

Seth D. Martin[1]

[1]*Department of Astronomy, University of Massachusetts, Amherst, MA, 01003 USA*

ABSTRACT

We collect BVR photometry for the open star cluster NGC-7789 using a 16" Schmidt Cassegrain telscope equipped with a 2k x 3k CCD that provides 15' x 24' field of view. We reduce our images with standard calibration techniques using bias frames, dark frames, and flatfields, and align and stack all of our exposures in each filter. We extract photometry from our processed images, and calibrate measurements of apparent magnitude using aperture photometry with a zero point calculated using GD-246 as our standard star. We then construct multiple color-magnitude diagrams of our stellar population and compare them to stellar isochrones. By visual analysis of the shape and offset between the CMD of our sample and the set of isochrones we employ, we estimate the age of NGC-7789 at 1 Gyr, and its distance from Earth at 2.49 ± 1 kpc. We use our derived distance to calculate monochromatic luminosites, and fit our stellar spectra to a product of surface area/solid angle and spectral radiance according to Planck's Law for emitting black bodies. We find that our derived temperatures and luminosities are high in error; we attribute this in part to a degeneracy in the scale of the spectra as it is affected by both temperature and surface area. We also note that fitting stellar spectra to merely 3 pass bands is likely insufficient to reliable trace the shape and therefore, precisely calculate the temperature of stars.

1. INTRODUCTION

The Hertzsprung-Russell (H-R) diagram is an invaluable tool for characterizing populations of stars. An H-R diagram is a simple a plot of temperature vs. luminosity, but it provides a wealth of potential information. Generally, temperature is displayed on the x-axis and is inverted to place hotter objects more to the left. Luminosity is then on the y-axis, and often uses solar units ($M_*/M_\odot$). The most prominent feature on an H-R diagram is the main sequence; this is where all stars, from the smallest to the most massive, will spend $\sim 90\%$ of their existence. This strip reaches from the hot-bright corner of the H-R diagram, for massive stars up to around 100 times the mass of the Sun, to the dimmer and fainter end, where the smallest objects that can still be considered stars (~ 0.08 solar masses) reside. Also of note are red giants, a post-main sequence phase where stars swell up and their surface cools, making them highly luminous and, as the name entails, red. The final step in a star's evolution will be either a white dwarf, a neutron star, or a stellar black hole, in increasing order of initial stellar mass. While white dwarfs will be visible in the hot and dim corner of the H-R diagram, but neutron stars and black holes generally drop out of the displayed region of the plot as they are simply too dim.

Based on these evolutionary stages, the age of a stellar population can be ascertained by examining its H-R diagram. Young star clusters will have bright, blue, type O main sequence stars, but these objects only last $\sim 10^8$ years before quickly transitioning to red giant territory. Smaller stars take longer to exhaust their hydrogen cores, so as a population ages, it will display a turnoff point that recedes down the main sequence. A Sun-like star has a lifetime of $\sim 10^{10}$ years, meaning that the oldest star clusters will peel off the main sequence just below where the Sun lies. Star clusters generally form around the same time, so the age of a star at the turn off point gives an estimate of the age of the cluster as a whole.

Luminosity and temperature cannot be measured directly by a telescope, rather, we can measure the apparent brightness from our location on Earth. If we construct a diagram with the color (difference in apparent magnitudes for different filters) on one axis and the apparent magnitude in one filter on the other, we get the color magnitude diagram (CMD). While the color magnitude diagram is analogous to the H-R diagram, they are not exactly the same. The spectra of stars generally resembles a black body emitter, with the presence of some emission and absorption lines from metals and cool H and He in the star's atmosphere. This means that its spectrum, or flux density as a function of wave-

length, can be described by a Planck function, for some effective temperature. Taking multiple measurements of monochromatic flux at different wavelengths allows a star's spectrum to be fitted to a Planck function for a specific temperature, which will be considered the star's effective surface temperature.

While effective surface temperature is indicative of the shape of the entire spectrum of a star, the color of two bands only samples the slope of the spectrum in one region, thus, the color indices of stars will change depending on which color is taken. Due to the nesting nature of the spectra of increasingly hot black bodies, colors taken with filters longward of the spectral peaks of the hottest objects will generally be bluer for hotter objects. As well, if we sample at longer wavelengths than the peak, the slope given by a color index in that regime uniquely determines the corresponding effective temperature. This is a consequence of the Rayleigh Jeans Law, an approximation that applies at the long wavelength regime of black body emissions. It simplifies the spectral radiance of a source to $B_\nu(T) = \frac{2\nu^2 kT}{c^2}$; if we take the derivative, the factor of T remains linear, therefore, the slope of a black body spectrum in the Rayleigh-Jeans tail is directly proportional to the temperature. Since color index is a measurement of the slope, this means that colors taken in long wavelength bands will directly correspond to effective black body temperature. Due to the fact that stars in the same cluster will all be similar distances to Earth, the ordering of sources by apparent magnitudes will not change much from the ordering by absolute magnitude or luminosity. Therefore, we can extrapolate much of the same information from a color-magnitude diagram as we can from an H-R diagram.

CMD's are particularly useful as an interstitial product in the process of creating an H-R diagram, if they are combined with another device: isochrones. An isochrone represents the regions of an CMD or H-R diagram occupied by stars of varying masses for a specific age and metallicity (simply the mass fraction of non-hydrogen/helium matter). Isochrones are created by creating analytical models for stars, using the equations that govern stellar structure, such as hydrostatic equilibrium, and solving them for stars at a particular age, then reporting the output spectrum of each simulated star. Isochrones in CMD form, however, are not reported in apparent magnitudes, but absolute magnitudes. With the absolute magnitude defined as the apparent magnitude of a source from a fixed 10-parsec distance, the difference between apparent and absolute magnitude results in the distance modulus: $m - M = 5log_{10}(\frac{d}{10pc})$. Therefore, one can fit the CMD of a stellar population to an isochrone for the appropriate age, and the necessary

shift on the magnitude axis will betray the distance to the cluster. By comparing the main-sequence turn-off point and the relative population of late stage objects such as red giants and short lived objects such as blue giants, we can match the shapes of CMD's to isochrones of varying age, and find that the best-fitting isochrone will be representative (though not necessarily precisely) of a star cluster's age. When fitting isochrones, one may also note that a horizontal shift is required to fit to the data. Often this is the result of dust extinction, causing the observe colors of a stellar population to redden, meaning the isochrone colors must be reddened as well.

The luminosity of a star is obtained by making a conversion from flux. Since flux is the light power received per unit of area, and light propagates in a spherical front from an isolated point source, the ratio of luminosity and flux is given by the surface area of a sphere with the same radius as an observer's distance to the source: $\frac{L}{F} = 4\pi d^2$. Our telescopes measure flux, so we must simply determine the distance to a star in order to derive its luminosity.

In general, there are two types of star clusters: open and globular. Globular clusters are older populations that tend to reside in remote regions of the galactic halo. Due to their ages (commonly $> 1 - 10+$ Gyr), the CMD of globular clusters tends to be devoid of massive main sequence stars. Instead, they will exhibit a turn off nearer to the middle of the main sequence, approaching Sun-like stars, as well as a highly populated red giant branch, and a small, difficult to measure population of white dwarfs. Their name comes from the fact that their stars are tightly bound by gravity, and thus tend to group together in close proximity. This makes them a difficult target for observation when resolution is limited, since it may be impossible to tell nearby stars apart. Open clusters, on the other hand, are more loosely bound clusters found primarily in the galactic disk. They are typically younger populations ($.1 - 1$ Gyr), housing larger numbers of massive, blue main sequence stars; this is a consequence of the fact that open clusters are not gravitationally bound, so they tend to dissipate rather than reach older ages. This does make them a better target for observation since their more diffuse distribution of stars can be more easily differentiated, even with lower angular resolution. The CMD or H-R diagram of open clusters will contain a more complete main sequence, as even the more massive stars may not have aged enough to evolve into giants. As a consequence, the red giant branch will be underpopulated, and end stage white dwarfs will be entirely absent, or very few in number.

2. METHODS

Our data are collected at the Smith College observatory, using the Meade LX200 ACF Schmidt-Cassegrain with a 16" primary mirror. A Cassegrain telescope is a reflector telescope configured with a hole in the center of the primary mirror, through which light collected in the secondary mirror is directed. The inclusion of a Schmidt corrector allows the telescope to use a spherical reflector with reduced aberration, lowering the cost of production while maintaining instrument quality. The telescope rests on an equatorial mount and is housed in a dome, both of which are driveable with computer software. The equatorial mount aligns one axis with our latitude (42.3°), allowing the apparatus to track objects against the rotation of the Earth by simply rotating on the right ascension (RA) axis. Our detector is a 2047 x 3072 pixel charge coupled device (CCD) with a UBVRI filter wheel and liquid nitrogen cooling; both of these features are also operable from a computer. The CCD was kept at around -30.1 °C. A CCD counts the electrons in each of its pixels produced by the photoelectric effect from incoming photons. Each pixel of the detector covers 0.5", giving a 15' x 24' field of view.

Observations took place on the night of October 27 2022. On that night, the weather was mostly clear, with few to no clouds and no precipitation. The atmospheric temperature was $\sim$ 12 °C, and humidity was $\sim$ 96%. We focused the telescope and used an unspecified star to determine seeing. From the full width at half maximum (FWHM) of the star in a test image, we determine the seeing to be 3.5". We took twilight flatfields at the beginning of our session, around 18:30 local time, as the Sun was setting. Observations of GD-246, our standard star, began at 20:17 local time (21:49 LMST), at which point the target was at an airmass value of 1.24. We started observing NGC-7789 at 20:46 local time (22:21 LMST), at airmass value 1.07 (see Table 1).

2.1. Data Reduction

The images we take through a telescope are contaminated with noise from a variety of internal and external sources. While external noise is a fact we must accept about our data, we can account for noise intrinsic to the instruments of observation. We construct 3 types of calibration frames: bias, dark, and flatfield, that each account for different sources of noise in our telescope-detector system. While we did take twilight flats prior to observations, due to time constraints we received bias and dark frames from the planetary transit team who used the observatory after us.
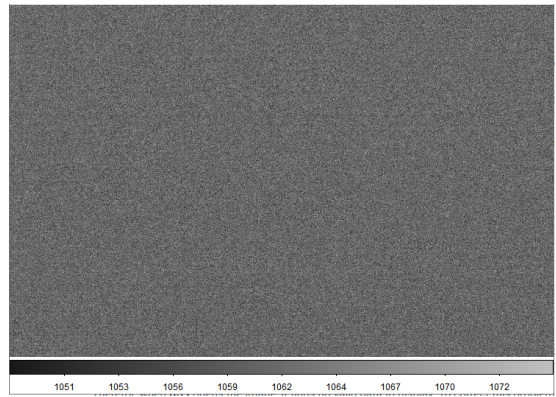
2.1.1. Bias Frames

Figure 1. Stacked bias frame made by median combining 10 bias images. The median pixel value in this image is 1061, with a standard deviation of 3.4.

To begin data reduction, we use the bias and dark frames taken by the transit team, some time after our observing session. We start with the bias frames, 0 second exposures with closed shutter used to measure noise produced by the detector as it reads pixel values. We stack 10 bias frames by taking the median pixel value over each pixel, producing a master bias frame. The need for bias frames arises from the bias voltage built into CCDs. Since the detectors need to process counts in as little memory as possible, negative numbers are undesirable (adding a sign infringes on the 16-bits allocated to pixel counts that allow a range of 0-65535). The bias voltage generally boosts pixel counts by $\sim$ 1000 ADU, and while it is generally consistent from frame to frame, small variations in counting still make stacking bias frames beneficial. Bias frames can also assess read-noise, which occurs due to the detector's own counting mechanism. This, again, will generally be present in every frame, regardless of exposure time.

2.1.2. Dark Frames

Dark frames are closed shutter exposures with non-zero exposure times, used to measure noise produced by thermal radiation inside the detector. Our 10 bias frames each use an exposure time of 60 seconds. We subtract the master bias values from each dark frame, then stack the bias-subtracted dark frames by similarly taking a median along each pixel location. This produces a master dark frame. Dark frames allow us to account for the electron counts originating from dark current, or thermal emissions. During any normal exposure, thermal photons will be captured to an extent determined by exposure time. As a result, it is generally best to use dark frames of similar or identical exposure times to science images, as the accumulation rate will then be more similar. Because the exposure time is now non-zero, as opposed to bias frames, we encounter

Table 1. Details of observation for our star cluster and standard star, as well as our calibration images

Target	Filter	RA (J2000)	Dec (J2000)	Exp. Time [s]	No. of Exp.	Total Int. Time [s]
GD-246	B	23:12:21	+10° 47' 4"	120	3	360
GD-246	V	23:12:21	+10° 47' 4"	120	3	360
GD-246	R	23:12:21	+10° 47' 4"	120	3	360
NGC-7789	B	23:57:29	+56° 43' 16"	180	8	1440
NGC-7789	V	23:57:29	+56° 43' 16"	60	8	480
NGC-7789	R	23:57:29	+56° 43' 16"	30	8	240
Twilight flat	B	∼ 23:00:00	∼ +10°	20	3	60
Twilight flat	V	∼ 23:00:00	∼ +10°	20	3	60
Twilight flat	R	∼ 23:00:00	∼ +10°	20	3	60
Bias frame	-	-	-	0	10	0
Dark frame	-	-	-	60	10	600

the possibility of capturing cosmic rays; but due to the stochastic nature of such interactions, stacking over median pixel values is generally sufficient to remove them. In our master dark frame, we note the presence of randomly distributed bright pixels. These same bright pixels are noticeable in our raw science frames, so these dark frames allow the same features to be subtracted out during the calibration process of our main images. We can see that the values of these pixels actually scale linearly with exposure time (for example, a particularly bright one near the top of the frame contains ∼ 7000) counts in our master dark, and ∼ 21000 counts in our 1st B band raw exposure of NGC-7789; there are no bright sources in the immediate region.) meaning these pixels are likely hot spots for thermal radiation in the detector.

2.1.3. *Flatfield Frames*

Finally, we calibrate the flatfield images. These are taken with an open shutter, pointed towards a diffuse light source, used to gauge the telescope's response to actual light over each pixel. Imperfections and dust inside the telescope, filter set, and the detector itself produce noticeable features in flat frames. These are most often dust particles housed within the telescope body, and due to being out of focus, appear in the shape of the mirror. For our Cassegrain style mirror, featuring a central cavity into which the secondary reflector is oriented, our flatfields feature rings distributed throughout the image. As well, since flatfields assess the relative pixel response, we can account for effects such as vignetting, which causes the edges of the image to darken. Flat frames must be taken separately in each band, so we take 3×20 second exposures in each band. This was done using the twilight sky as a light source, so we point the telescope at RA: ∼ 23h, Dec: ∼ 10° at 18:30 local
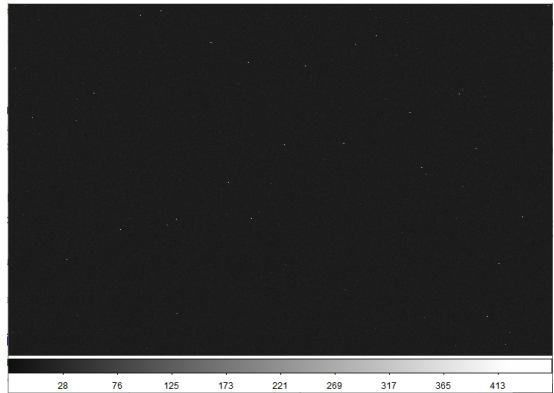

Figure 2. Master dark frame, composed of 10 bias subtracted dark frames taken at 60s exposure times. Here, the median pixel value is 6, with a standard deviation of 26. This means that dark current noise is generally smaller than bias counts, but more varied. The stray bright pixels persist over a median stack, meaning they are not simple transient anomalies, such as cosmic rays, that are unlikely to occur in the same location with enough consistency to contaminate a median stack.

time. Assuming the telescope is pointed far enough away from the setting sun, the twilight sky will be a diffuse enough source to measure flatfields with, and will not be as bright as the daytime sky, so as to saturate the detector with short exposures. From the flatfield images, we must then subtract the master bias and dark frames, but the master dark is scaled to match the exposure time of the flatfield. Each flatfield is then normalized by dividing itself by its own median pixel value. This converts each flatfield from an absolute scale, corresponding to an arbitrary brightness and exposure time, to a relative scale, which can then be used for any exposure of bright sources to normalize the pixel response across the image. We median combine the flats just as we did with
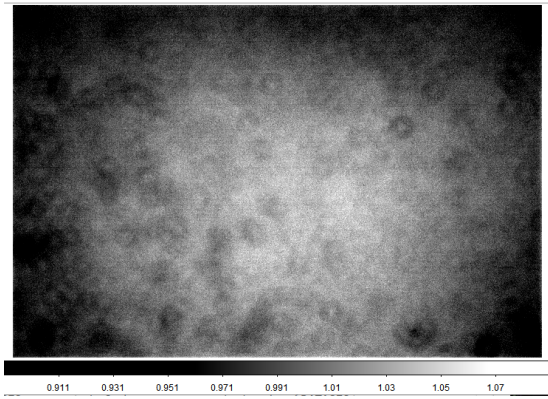
Figure 3. Stacked, calibrated, and normalized flatfield taken in B band. Since the image is normalized, the median is naturally unity (to 2 decimals); the minimum and maximum are 0.9 and 1.09, meaning the largest fluctuations are around 10% from the median. Meanwhile, the raw twilight flats for B band have pixel values ranging 20000-40000 as we aim to keep these measurements within the linear regime of detector response.

the bias and dark frames, and produce master flatfields for B, V, and R bands.

2.1.4. *Calibration of Science Images*

We calibrate our standard star and star cluster images in a similar fashion. We first subtract the master bias frame, then subtract the master dark frame, scaled to the ration of exposure times between the image in question and the master dark. To calibrate with the flatfield, we simply divide the image by the master flat frame in the appropriate band, since the flat frames are normalized. When we divide by the flatfield, since it is normalized to unity, regions with darkening will have values less than 1, and brighter regions will have values greater than 1. The same gradient will be present in any observing frames, so dividing out he flatfield "flattens" the pixel sensitivity across the frame and rids the image of darkening effects from dust rings and vignette.

2.2. *Alignment and Stacking*

Next, we stack the newly calibrated science images. We first identify one image of our set to be used as a reference for alignment. For both our standard star and star cluster image sets, we choose the first exposure in the B band as the reference. We then identify, in each reference image, an isolated point source, and a nearby patch of empty sky. We select around both, a 50x50 pixel box to use for centroiding. We take the empty sky sub-frame to sample the background noise, by taking its median and standard deviation in pixel values. In the sub-frame containing our point source, we identify all pixels exceeding 3 standard deviations

above the median noise value. We take only these pixels, subtract the noise from their pixel values, and take a light-weighted mean position. Similarly to locating a center of mass, we multiply a pixel's value with its x,y coordinates (separately) and sum upon the products. The sum is divided by the total pixel count in the region (remembering that background pixels are being ignored), and this provides the centroid pixel coordinates. By comparing these coordinates in different images, we can account for misalignment as the telescope's tracking software is not exact, and results in a drift of $\lesssim 10$ pixels over the course of our exposures. We roll each image by its x and y coordinate shifts from the reference image centroid coordinates, and pad the edges with 50 NaN pixels on each side. These shifted images can then be stacked, and trimmed (by the maximum pixel drift on each axis), producing fully calibrated, stacked images in each band, for each object. This results in 3 images per object, one for B, V, and R bands. Stacking images allows us to improve the signal to noise ratio (SNR) of our data by combining multiple images of the same field. Longer exposures are not always possible, since bright objects will eventually saturate, so we use stacking to improve the SNR, particularly for fainter objects. Since the source pixel values for a faint object will be closer to the noise values, it can become unclear whether a pixel in the vicinity of a source is part of the source, and displaying a statistical deviation towards the low end, or a high fluctuation in the noise. By combining multiple aligned images through a median stack, those fluctuations in both the noise and the source are diminished, and sources become clearer, and more defined, while the noise values become somewhat less varied.

2.3. *Source Extraction*

We can now extract photometric data from our star cluster images. The first step is source extraction, in which we define what groupings of pixels constitute stars, then count the total pixel value in that group and account for noise. To do this, we first examine our images visually to estimate two pieces of information: 1. full width at half maximum (FWHM) of a typical source; 2. desired SNR of selected sources. We examine our images and determine the characteristic FWHM to be around 7-8 pixels, and set the SNR minimum to 25. We then use the python package photutils with these settings, and we extract source locations from our B band images, for both our cluster and standard fields. We find 578 stars in our NGC-7789 images, and use the B band locations for photometry in all filters. Decreasing the SNR cutoff does increase our number of sources; using a FWHM of 10 pixels and a SNR limit of 20, we can

recover up to 905 for our B band image of NGC-7789, and we also note that the longer wavelength bands progressively produce fewer source counts for the same SNR cutoff and FWHM.

2.4. *Aperture Photometry*

Performing aperture photometry on the extracted sources requires first that we establish an aperture radius. A circle of this radius centered on the centroid location of a source is used to count the total value of source pixels. We then define a sky annulus, which is a ring outside of the aperture which is used to sample background noise in the vicinity of a source. We take the median pixel value in our sky annulus, and divide by the total number of pixels in the annulus, giving us the area density of sky noise. We then multiply this value by the area of the aperture, estimating the sky noise contained in the aperture. The corrected aperture pixel count is then derived by subtracting the sky noise per pixel times the number of pixels in the aperture from the raw aperture pixel count. We must also divide the source pixel counts by exposure time, since flux includes a per unit time aspect. This instrumental flux, F_{inst} allows us to calculate instrumental magnitudes as $m_{inst} = -2.5log_{10}(F_{inst})$. Instrumental magnitudes simply convert instrumental flux counts into magnitude scale, which we can later use to find calibrated apparent magnitudes. We derive measurements of flux per unit time for our sources, along with errors, using 10 pixel apertures and sky annuli with a 15 pixel inner radius and 20 pixel outer radius. We again use the python package photutils to take our source coordinates and measure flux counts and sky noise at each location.

2.5. *Flux Calibration*

In order to measure the brightness of stars in our target star cluster, we need a reference star with known brightness, a standard star, since the telescope CCD measures ADU (analog to digital units, sometimes referred to with other names, but this is essentially an arbitrarily scaled number corresponding to the electrons counted in each pixel) and not actual photons/photon energies. The target units are magnitudes, a log-scaled analog to flux/flux density with units of power per unit area (per unit frequency/wavelength for flux density). Our standard star is GD-246, and we determine its location in our standard star images using Aladdin-Lite (Figure 4) and comparing its position to other nearby sources. We also look up its official B, V, R magnitudes on Simbad. We can calculate an instrumental magnitude for GD-246 by taking $-2.5log_{10}(F_{inst})$ and if we subtract this value from the official value in each

band, we derive the zeropoint for each filter. We find the B, V, R, zeropoints are 19.82 ± 0.005, 20.11 ± 0.006, and $20.16 \pm .007$, respectively (see Table 2). Adding the zeropoint for a filter to a source's instrumental magnitude in that filter gives us the apparent magnitude of that source. We calculate instrumental magnitudes for the remainder of our sources and convert them to apparent magnitudes using this formula. We determine uncertainties in our zeropoints by adding in quadrature, the listed errors in the standardized magnitudes, and the error in instrumental magnitudes, propagated by $\sigma_{m,inst} = 2.5 * 0.434\frac{\sigma_{F,inst}}{F_{inst}}$. When we calibrate our fluxes using the zero points, the function is again, a simple addition, so we add the zero point uncertainties to instrumental magnitude errors in quadrature as well.

3. ANALYSIS

3.1. *Isochrone Fit*

We take our newly derived photometric catalog for NGC-7789, and plot 3 color-magnitude diagrams, using each band as the vertical axis for one CMD, and using all 3 possible colors (Figure 5). We take isochrones from Marigo et al. (2008) to further analyze our stellar population using these CMDs. We determine the best fit to the population is the 1 Gyr isochrone, and discard the others. This is done simply by plotting the full set of isochrones alongside the cluster CMD, and comparing the shapes to see which age isochrone best matches the cluster's distribution in color-magnitude space. The set of isochrones includes only 6 ages, ranging from 10 million, to 10 billion years. As such, our best fit isochrone does not determine the cluster's age precisely, rather, it implies that the age of NGC-7789 is nearer to 1 Gyr than either of the adjacent isochrone ages (300 Myr and 10 Gyr; we can only estimate that our uncertainty in this value is around 0.5 orders of magnitude). Since the isochrones report photometric values in absolute magnitudes, we must shift them on the vertical axis to meet our data. By matching each of the 3 CMDs, we find 3 similar, but varying vertical shifts. Since these shifts correspond to the distance modulus, we take their mean and standard deviation, and add a 0.25 magnitude visual uncertainty in quadrature, then calculate the distance, propagating uncertainty through a simple Monte Carlo simulation with 10^5 draws. We find the distance to NGC-7789 is 2.49 ± 1 kpc. We also note that there are horizontal shifts applied, particularly to the V vs. V-R plot, which required a slight redshift of 0.15 magnitudes. While the other two CMDs do not agree with a reddening adjustment, we also note that the V vs. V-R is our best fit to the isochrone model, so it is most likely that some dust attenuation is at play in our observations.

Table 2. Flux calibration values for our standard star, GD-246. We use apparent magnitudes measured by Landolt (2009) to determine zero points.

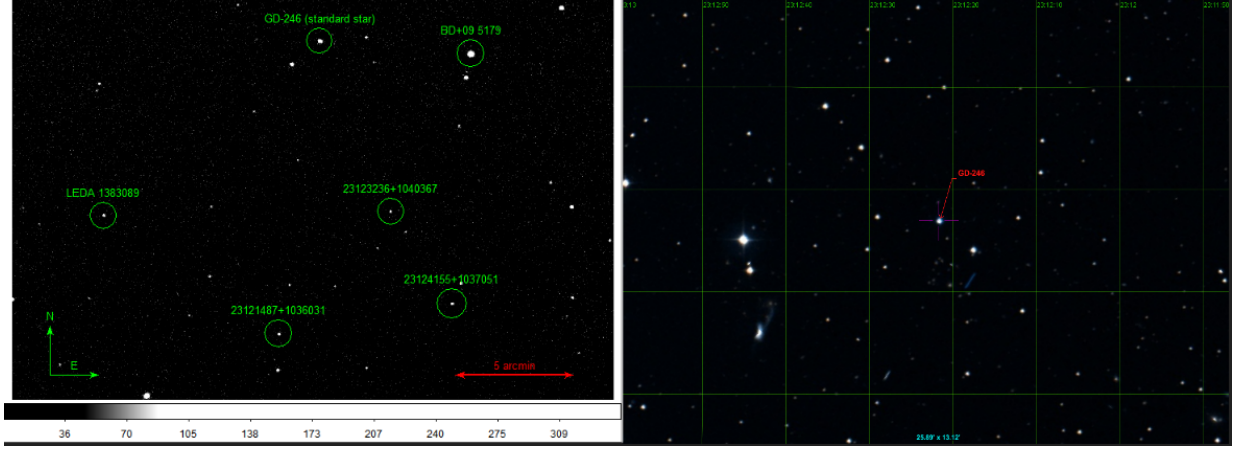| Target	Filter	Catalog value	Instrumental magnitude	Zero point
GD-246	B	12.772 ± 0.0009	-7.04 ± 0.005	19.82 ± 0.005
GD-246	V	13.090 ± 0.0009	-7.02 ± 0.006	20.11 ± 0.006
GD-246	R	13.238 ± 0.0009	-6.91 ± 0.007	20.16 ± 0.007

Figure 4. (Left) Our standard star field, with sources labeled to help identify our target, GD-246. We construct this diagram by comparing our processed image in B band with SIMBAD and 2MASS objects shown in Aladin-Lite. (Right) Aladin DSS2 color image of the same region of sky. Note that while North is the same between both images, the Aladin image is mirrored, and East is to the left of the image.
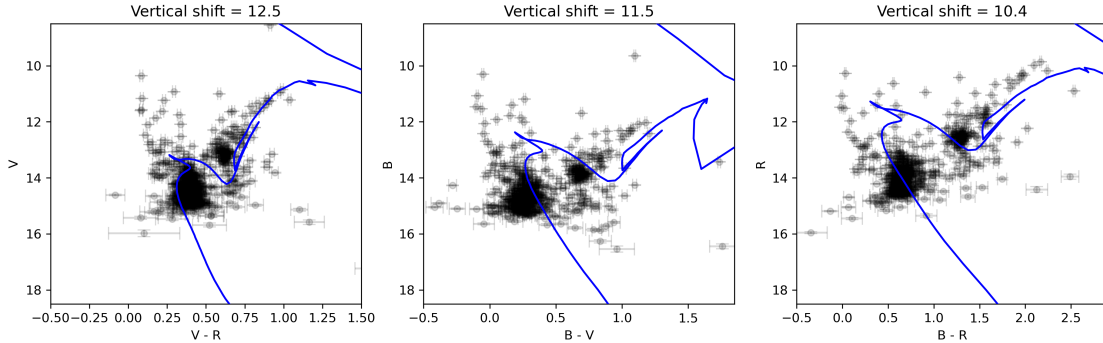

Figure 5. Color-magnitude diagrams of NGC-7789. The blue line in each panel is the Marigo et al. (2008) isochrone for a 1 Gyr stellar population, and we shift the photometry to match the isochrones. The vertical shift for each panel is the value we subtract from the apparent magnitudes of our objects to match them to the position of the isochrone; this is also the distance modulus we use to estimate the distance to NGC-7789. These are significantly varied because only the V vs. V-R plot matches the isochrone well.

3.2. SED Fitting

Deriving the distance to the star cluster enables us to directly construct the parameters for an H-R diagram: temperature and luminosity. At present, our magnitudes are still relative to Vega, so we begin by making the correction from Vega magnitudes to AB magnitudes. This is a simple linear shift that depends on the filter; for B, V, and R bands, the differences of AB and Vega magnitudes are -.09, .02, and 0.21, respectively. The next step is to convert into flux density, using the relation: $m_{AB} = 8.9 - 2.5log_{10}(F_\nu[Jy])$. We then derive monochromatic luminosities as $L_\nu(\nu_a) = 4\pi D^2 * 10^{(m_a+c_a-8.9)/-2.5} * 10^{-26}$ where the factor of 10^{-26} we apply is simply to convert from Jy to $\frac{W}{m^2 Hz}$.
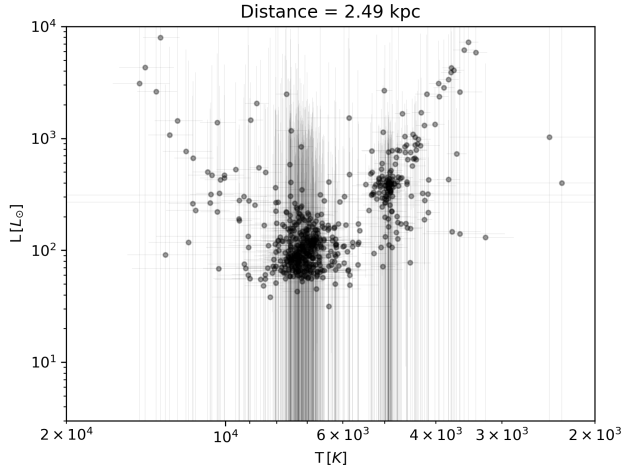
Figure 6. H-R diagram for NGC-7789. The large errors on certain objects as well as the significant offset from the expected luminosities of such a stellar population are indicative of limitations on our data set as well as potentially in our analysis techniques. Still, we derive reasonable estimates of temperature and luminosity for this stellar population.

We must also note the central wavelengths of our 3 band passes; B: 445 nm, V: 551 nm, R: 658 nm. These values construct optical spectral energy distributions (SEDs) to which we can fit model spectra.

We now employ the relation between monochromatic luminosity and spectral radiance: $L_\nu(\nu_a) = 4\pi^2 R^2 * B(\nu_a, T)$. Since the spectra of stars resemble closely those of perfect blackbodies, we can use Planck's law to model stellar spectra. Planck's law defines the spectral radiance at every wavelength or frequency in accordance to on objects surface temperature: $B_{nu}(\nu, T) = \frac{2h\nu^3}{c^2} \frac{1}{e^{\frac{h\nu}{kT}} - 1}$ in SI units of $\frac{W}{m^2 \, Hz \, sr}$. We define a function that evaluates Planck's law for a given wavelength and temperature, multiplied by a factor of $4\pi^2 R^2$ to return luminosity density. We then perform a simple curve fitting for each objects luminosity spectrum, and derive a best fit temperature and radius.

To test the efficacy of this fitting method, we acquire solar photometry in AB magnitudes from Willmer (2018). Using the aforementioned methods to derive monochromatic luminosity and fit the spectrum, we produce the best fit parameters for the surface temperature and radius of the Sun. We find $T_\odot = 5830$ K and $R_\odot = 680000$ km; as we fall well within 10% of the accepted values for both, we establish that our fitting procedure works, at least given high quality photometry and well measured distances.

Using the distance we derived from the CMD and isochrones, we proceed to derive temperatures and radii

for our entire star cluster sample. With these, it is trivial to determine luminosities, given the Stefan-Boltzmann Law: $L_{bol} = 4\pi R^2 \sigma T^4$. We plot the resulting H-R diagram and find that it displays a turn off from the main sequence around 100 $L_\odot$ and roughly 6000 K (Figure 6). Since the stellar population we are observing is around 1 Gyr in age, we expect the stars now reaching the end of their main sequence life to be significantly more massive than the Sun, and consequently, hotter, larger, and brighter. Still, we note large errors in the fainter objects, which are also those nearest to this pivot point, and attribute those to imprecisely derived parameters (i.e. our distance modulus, which was measured by eye). Furthermore, since we fit the spectra to merely 3 bandpasses, we do not necessarily constrain the shape of the spectra as well as possible. There is also a degeneracy in our fit, coming from the fact that increasing temperature and radius will both increase brightness at all wavelengths; therefore, the scaling factor between spectral radiance and monochromatic luminosity is affected by both parameters, and is less able to constrain either one. Were we able to acquire upwards of 5 filters worth of photometric observations, as well as to more accurately measure the distance to NGC-7789, we may have been able to more rigorously define the temperatures and luminosities of our sample.

4. CONCLUSION

Using BVR photometry taken from Smith College's 16" Schmidt-Cassegrain telescope, we are able to construct CMDs of the stellar population of NGC-7789. Through these CMDs, we estimate the distance and age of the cluster to be 2.49 ± 1 kpc and $1(-0.7 + 3)$ Gyr. The currently accepted age of NGC-7789 is 1.70 Gyr, and it is measured to be 2.34 kpc from the Solar System ((Kharchenko et al. 2005)). While our uncertainties are large due to the imprecise nature of visual isochrone fitting, we are with 10% of the true distance, and measure the nearest isochrone age to truth. If we apply the Kharchenko et al. (2005) value of distance to our luminosity calculations, the modeled luminosities of our sample drop by nearly an order of magnitude. If we can model the shape of the spectra with more data, we may be able to pin down temperature with enough certainty to break the degeneracy in the model and find more reasonable luminosities. There are other shortcomings in the model, such as the assumption of perfectly isotropic radiation, the omission of absorption and emission features, and the assumption of emissivity equal to unity. Accounting for these would increase the number of free parameters in the model, thus, we would be presented with further degeneracies to break, and not

enough data. We also note that our SNR restriction for source extraction was quite strict, and likely limited our dynamic range of apparent magnitudes. One consequence of this is our CMD's main sequence being less complete at fainter magnitudes. This makes the overall shape harder to gauge and limits the efficiency of our visual isochrone fit, therefore increasing the uncertainty in our extrapolated distance and age for the star cluster.

REFERENCES

Kharchenko, N. V., Piskunov, A. E., Röser, S., Schilbach, E., & Scholz, R. D. 2005, A&A, 438, 1163, doi: 10.1051/0004-6361:20042523

Landolt, A. U. 2009, AJ, 137, 4186, doi: 10.1088/0004-6256/137/5/4186

Marigo, P., Girardi, L., Bressan, A., et al. 2008, A&A, 482, 883, doi: 10.1051/0004-6361:20078467

Willmer, C. N. A. 2018, The Astrophysical Journal Supplement Series, 236, 47, doi: 10.3847/1538-4365/aabfdf